

Unified understanding of the first-order nature of the transition in TbCo₂

Chao Zhou ^{1,*}, Tiejian Chang,² Zhiyong Dai,¹ Yuanliang Chen ¹, Chenyang Guo,¹ Yoshitaka Matsushita ³, Xiaoqin Ke,¹ Adil Murtaza,¹ Yin Zhang,¹ Fanghua Tian,¹ Wenliang Zuo,¹ Yu-sheng Chen,² Sen Yang ^{1,†} and Xiaobing Ren⁴

¹*School of Physics, MOE Key Laboratory for Nonequilibrium Synthesis and Modulation of Condensed Matter, Xi'an Jiaotong University, Xi'an 710049, China*

²*NSF's ChemMatCARS, The University of Chicago, Lemont, Illinois 60439, USA*

³*National Institute for Materials Science, Beamline BL15XU, Spring-8, 1-1-1 Kohto, Sayo-cho, Hyogo 679-5148, Japan*

⁴*Center for Functional Materials, National Institute for Materials Science, Tsukuba, Ibaraki 305-0047, Japan*



(Received 27 April 2022; accepted 20 July 2022; published 5 August 2022)

The determination of the nature of phase transitions, especially those that involve two symmetry-breaking order parameters, is a fundamental issue in condensed matter physics. For the Laves-phase rare-earth-transition-metal intermetallic compounds, their phase transitions involve both magnetic ordering and structural ordering. As a typical material of the Laves-phase intermetallics, TbCo₂ has been studied extensively for its transition around 230 K. However, the understanding on the nature of this transition has remained controversial (first/second order) for decades. Here, in this paper, based on the criteria that determine first-order and second-order transitions for magnetic materials, which are (1) latent heat, (2) thermal hysteresis, (3) coexistence of phases, and (4) the Banerjee criterion, we show direct evidence to reveal the first-order nature of the transition in TbCo₂, which is further interpreted by a Landau theory based phenomenological approach. Our work reconciles the lasting arguments on the transition of TbCo₂ and may pave the way for deepening the understanding on the transitions of magnetic materials that involve both magnetic and structural transitions.

DOI: [10.1103/PhysRevB.106.064409](https://doi.org/10.1103/PhysRevB.106.064409)

I. INTRODUCTION

Phase transitions are at the foundation of magnetic functional materials, in particular the ones that involve the symmetry breaking of more than one order parameter [1]. The relationship between such transitions and functionalities is well exemplified by Laves-phase rare-earth-transition-metal compounds RT_2 (R refers to rare-earth elements and T refers to transition-metal elements), which undergo a magnetic transition associated with a structural change [2].

Owing to the competition between the rare-earth-transition-metal exchange interaction and crystalline electric field effect [3,4], RT_2 alloys show diverse interesting effects, e.g., magnetostriction [5,6], magnetocaloricity [7,8], tunable thermal expansion [9], magnetoresistance [10,11], etc. Therefore, given the direct relationship between the transition and physical properties, it is crucial to investigate the nature (first/second order) of these phase transitions in view of both fundamental theory and application.

As one typical compound in the RT_2 family, TbCo₂ has been studied extensively on both magnetic transition and structural transition around 230 K. Early studies indicate that the transition of TbCo₂ is a second-order magnetic transition associated with a structural transition [12–17], which violates the common knowledge on the determination of the nature of the phase transition [18,19]. A recent study reported the

first-order nature of this transition, but pointed out that the magnetic transition and structural transition decouple [20], contradicting a wealth of experimental evidence [9,21–23]. In one word, the nature of the transition in TbCo₂ remains an open question of interest.

Experimentally, for magnetic materials, the criteria for determining second-order phase transition (SOPT) or first-order phase transition (FOPT) are (1) latent heat [14,24], (2) thermal hysteresis [14,24], (3) phase coexistence [25], and (4) the Banerjee criterion [26–29]. In this paper, based on the evidence from the above-mentioned experimental results, we show that the paramagnetic-ferrimagnetic transition in TbCo₂ is of first order.

II. EXPERIMENTS

The TbCo₂ alloy was prepared by the arc melting method with the raw materials of Tb (99.9%) and Co (99.9%) in an argon atmosphere. To ensure compositional homogeneity, the sample (about 8 g) was melted four times. The as-cast ingot was cut into slices of thickness 1 mm and sealed into a quartz tube filled with argon gas; then the sealed sample was annealed at 1273 K for 72 h, and naturally furnace-cooled to room temperature. Synchrotron x-ray diffraction (XRD) was carried out at the BL15XU NIMS beamline of Spring-8 with an x-ray wavelength $\lambda = 0.6538$ Å. The samples for synchrotron XRD were well-ground powders that were sealed into Kapton capillaries. The capillary was rotated during the measurement to reduce the preferred orientation effect and to average the intensity. The crystal structures were refined

*chao.zhou@xjtu.edu.cn

†yang.sen@xjtu.edu.cn

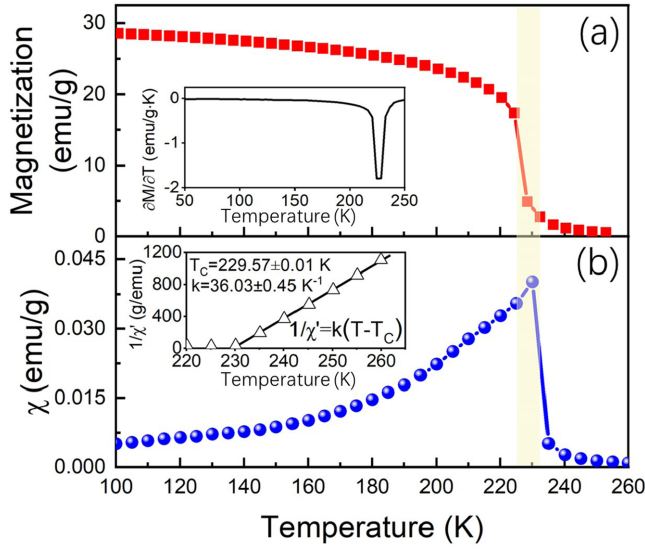


FIG. 1. (a) M - T curve and (b) χ - T curve of TbCo_2 . The derivative of magnetization over temperature and fitted $1/\chi'$ - T curve are shown in the insets of (a) and (b), respectively.

using the Rietveld algorithm [30,31]. The samples used for the physical property measurements are polycrystalline bulk. The heat flow on heating and cooling processes across the Curie temperature (T_C) is monitored using a differential scanning calorimeter (DSC, Q2000, TA Instruments). The magnetic measurements were performed on a superconducting quantum interference device (MPMS-SQUID, Quantum Design). The magnetization (M) versus temperature (T) curve was measured on cooling at a rate of 2 K/min from 260 to 100 K, under a field of 500 Oe. The magnetic susceptibility (χ) versus temperature (T) curve was measured on cooling at a rate of 2 K/min from 260 to 100 K, under a field of 2 Oe with a frequency of 133 Hz. Before the measurement of isotherm $M(H)$ curves, the magnet reset process was performed to make sure there would be no frozen field to influence the magnetization behavior at low field.

TABLE I. Crystal data and structure refinement for TbCo_2 at 130 K.

Wavelength	0.6538 Å		
Crystal system	Trigonal		
Space group	$R\bar{3}m$ (No. 166)		
Unit cell dimensions	$a = 5.0962(1)$ Å		
	$b = 5.0962(1)$ Å		
	$c = 12.5336(1)$ Å		
	$\alpha = 90^\circ$		
	$\beta = 90^\circ$		
	$\gamma = 120^\circ$		
Volume	281.905(2) Å ³		
Goodness of fit on F ²	0.925		
R indices (all data)	$R_p = 6.62\%$	$R_{wp} = 9.34\%$	
Atomic parameters			
Atom	Wyckoff	Position	Occ.
Tb	6c	0,0,0.1243	1
Co1	3b	0,0,0.5	1
Co2	9e	0.5,0,0	1

III. RESULTS AND DISCUSSION

Figure 1 shows the magnetization (M) versus temperature (T) and susceptibility (χ) versus temperature curves. From the $\partial M/\partial T$ - T [inset of Fig. 1(a)] curve and fitted $1/\chi'$ - T curve [inset of Fig. 1(b); the deduction of the fitting is given in the Supplemental Material [32]], T_C is determined as 229.57 ± 0.01 K, agreeing well with the reported values [9,20].

The XRD profile and refined pattern at 130 K (below T_C) are shown in Fig. 2(a), and the crystallographic information is listed in Table I. The refined XRD pattern reveals that in a ferrimagnetic state, TbCo_2 crystallizes in a rhombohedral structure with the space group $R\bar{3}m$ (No. 166).

The evolution of the crystal structure from above T_C to below T_C , as reflected by the evolution of the characteristic reflections $\{222\}$ and $\{800\}$ from 260 to 200 K observed from *in situ* synchrotron XRD measurements, is shown in Fig. 2(b1). At 260 K, no splitting in both $\{222\}$ and $\{800\}$

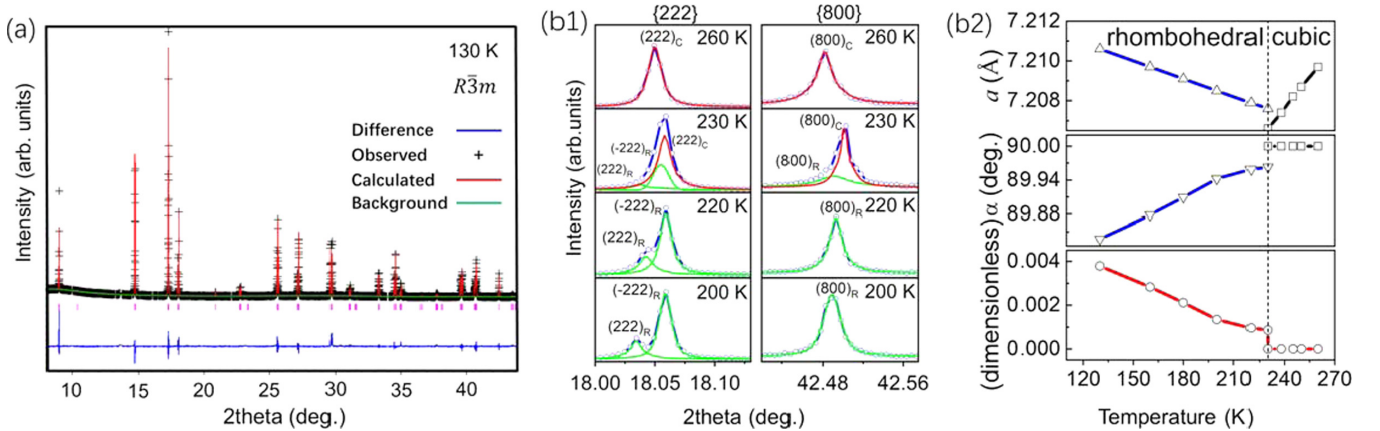


FIG. 2. (a) The refined XRD patterns for TbCo_2 at 130 K. The background and calculated Bragg peak positions are shown below the observed (plus) and calculated (red line) intensities, and the difference is shown by the blue line at the bottom. (b1) Characteristic XRD reflections $\{222\}$ and $\{800\}$ at 260, 230, 220, and 200 K, respectively, with the red, green, and blue lines denoting the cubic fit, rhombohedral fits, and full sum, respectively. (b2) Lattice parameters and lattice strain within the temperature range 130–260 K.

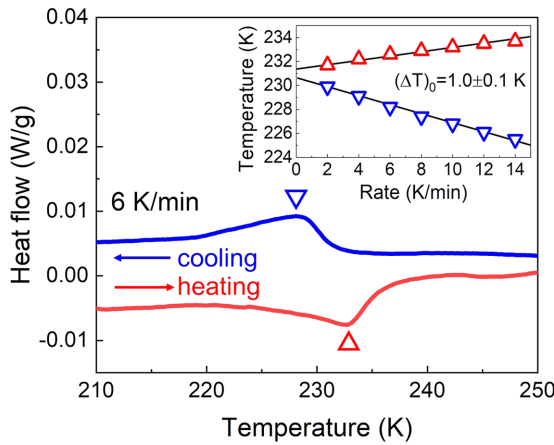


FIG. 3. Heat flow of TbCo_2 on heating and cooling processes at a rate of 6 K/min. The inset shows the ramp rate dependence (linear fitting) of exothermic and endothermic peak temperatures.

reflections is in accordance with the detected cubic crystal structure [21]. At 220 and 200 K, the splitting in the $\{222\}$ reflection and no splitting in the $\{800\}$ reflection indicate a rhombohedral crystal symmetry [33]. At 230 K, which is the detected magnetic transition temperature from the M - T curve [Fig. 1(a)] and χ - T curve [Fig. 1(b)], the asymmetric peak shape of the reflections $\{222\}$ and $\{800\}$, especially of $\{800\}$, is observed clearly, which indicates the phase-coexistence state. In addition, the asymmetric peaks are consistent with the superposition of cubic and rhombohedral profiles. Upon further cooling, the emergent splitting of the $\{222\}$ reflection below T_C unambiguously suggests a structure phase transition, and the observed phase coexistence at 230 K further proves the first-order nature of the transition. The calculated lattice parameters and spontaneous lattice strain ε (the calculation of ε can be found in Ref. [25]) are shown in Fig. 2(b2).

The DSC measurement was carried out to check the heat flow during the transition (Fig. 3). The appearance of an exothermic peak on the cooling process and the endothermic peak on the heating process proves a FOPT around 230 K. The temperatures of the exothermic peak and endothermic peak are 228 and 233 K (at a rate of 6 K/min), respectively, agreeing well with the magnetic transition temperature (Fig. 1). To eliminate the impact of temperature ramp rate, the rate dependence (2, 4, 6, 8, 10, 12, and 14 K/min) of the measured peak temperatures is investigated and presented in the inset of Fig. 3. Following the common treatment [34,35], linear fitting is adopted to fit the rate dependence. The magnitude of the thermal hysteresis is ~ 1 K at an extrapolated zero ramp rate, comparable to the value reported recently (0.6 K) [20]. The nonzero latent heat (DSC peak) and the thermal hysteresis both reveal the first-order nature of the transition around 230 K. It should be noted that the thermal hysteresis between the exothermic and endothermic peaks was previously detected but neglected, and thus the transition at ~ 230 K was incorrectly classified as a second-order magnetic transition associated with a structural change [13].

Since the transition in TbCo_2 has been regarded as second order for a long time, the theoretical models for SOPT, i.e., scaling hypothesis and Heisenberg model [13], were em-

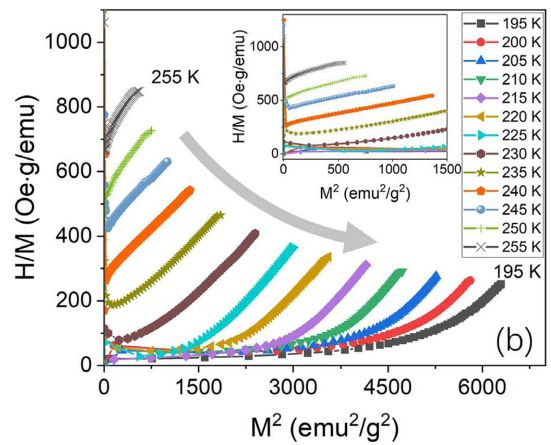
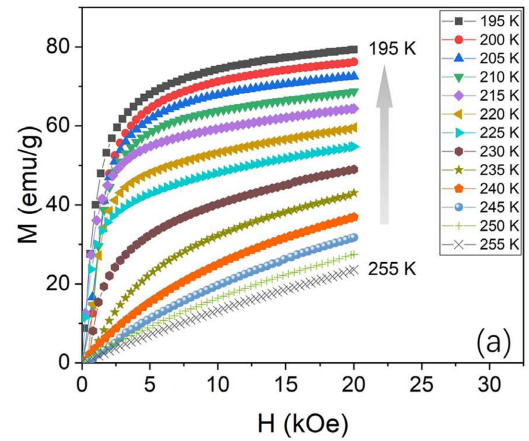


FIG. 4. (a) The magnetization isotherms measured at selected temperatures near T_C under an applied field of 2 T. (b) The isotherms of H/M - M^2 : The inset shows the curve of the low magnetization region.

ployed for investigating the transition. Here, in this paper, the nature of the transition of TbCo_2 is analyzed based on the Banerjee criterion [26].

Figure 4 shows the magnetization isotherms and the corresponding H/M - M^2 within the temperature range across T_C . From Fig. 4(a), it is seen that the change of magnetization from neighboring temperatures reaches a maximum at 230 K. The negative slopes of H/M - M^2 curves are observed in Fig. 4(b), demonstrating the FOPT according to Banerjee's criterion [36,37]. Attention should be paid to the negative slopes appearing in the low magnetization region [inset of Fig. 4(b)], where the data points might be missed if the measurement step of H is not small enough. This may explain why the Arrott plot method was used for TbCo_2 but the negative slopes were not observed [13,21,38].

An interesting fact is that many of the previously reported SOPTs of the magnetic materials have been revised to FOPTs in recent years, e.g., Fe, Ni, Co, CoFe_2O_4 , NdCo_2 , and PrCo_2 [14,24,39]. This is not difficult to understand, as we will show in the following by using a Landau phenomenological approach.

Under an applied magnetic field, the change in Gibbs free energy per unit of volume [see Eq. (S1) in the Supplemental

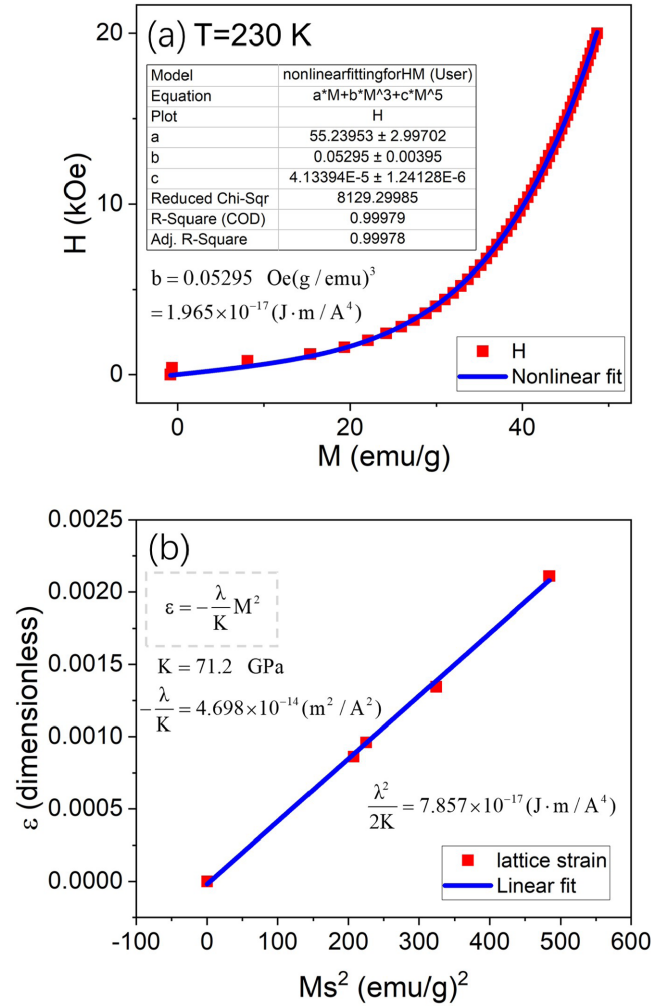


FIG. 5. (a) H vs M curve and nonlinear fitting. (b) Lattice strain ε vs M_s^2 and linear fitting. In (b), the values of M_s and ε are obtained from M - H loops and the synchrotron XRD patterns measured at 180, 200, 220, and 230 K; the value of K (71.2 GPa) is taken from Ref. [20].

Material [32]] is modified as [40]

$$\Delta G(M, H) = \frac{1}{2}a_0(T - T_C)M^2 + \frac{1}{4}bM^4 + \frac{1}{6}cM^6 - M \cdot H, \quad (1)$$

where H is the applied magnetic field.

The equilibrium condition $\partial \Delta G(M, H)/\partial M = 0$ leads to

$$H = a_0(T - T_C)M + bM^3 + cM^5. \quad (2)$$

Therefore, H and M follow the nonlinear relationship as Eq. (2) expresses. From the fitted curve [Fig. 5(a)], the value of b is calculated to be 1.965×10^{-17} (J m/A⁴).

For the materials where the structural transition and the magnetic transition occur synchronously, strong coupling exists between the two order parameters of magnetization (primary) and lattice strain (secondary) [25], as demonstrated in the case of TbCo₂ [41]. Then, the change of Gibbs free energy is rewritten as [24,25]

$$\Delta G(M, \varepsilon) = \frac{1}{2}a_0(T - T_C)M^2 + \frac{1}{4}bM^4 + \frac{1}{6}cM^6 + \frac{1}{2}K\varepsilon^2 + \lambda\varepsilon \cdot M^2, \quad (3)$$

where the elastic energy ($\frac{1}{2}K\varepsilon^2$) and the magnetoelastic coupling energy ($\lambda\varepsilon \cdot M^2$) are added, in which K is the elastic modulus, ε is the lattice strain, and λ is the coupling coefficient.

Minimizing the energy with respect to the strain [$\partial \Delta G(M, \varepsilon)/\partial \varepsilon = 0$] yields a relation between ε and M^2 :

$$\varepsilon = -\frac{\lambda}{K}M^2. \quad (4)$$

Substituting Eq. (4) into Eq. (3) leads to

$$\Delta G = \frac{1}{2}a_0(T - T_C)M^2 + \left(\frac{1}{4}b - \frac{\lambda^2}{2K}\right)M^4 + \frac{1}{6}cM^6. \quad (5)$$

Therefore, the order of the transition can be determined from the value of the coefficient of the fourth-order term ($\frac{b}{4} - \frac{\lambda^2}{2K}$) [28].

Based on the spontaneous magnetization [M_s , calculated using the law of approach to saturation (LAS) [42,43]] and lattice strain [ε , calculated from the XRD patterns in Fig. 2(b2)], the linear relation $\varepsilon \sim M_s^2$ is fitted as shown in Fig. 5(b). The value of $\lambda^2/2K$ is calculated to be 7.857×10^{-17} (J m/A⁴). As a result, the coefficient of the fourth-order term $\frac{b}{4} - \frac{\lambda^2}{2K} = -7.366 \times 10^{-17}$ (J m/A⁴) is small but indeed negative, suggesting a weak FOPT [44]. Such a conclusion is consistent with that obtained from Figs. 1–4.

Last but not least, it should be pointed out that the coupling of magnetization with the lattice strain, which results from the exchange interaction effect [45], would drive the magnetic ordering to become first order [2,46,47]. If the exchange interaction is admitted being a function of lattice interatomic spacing and the lattice is deformable, then the transition would become a FOPT, and yield latent heat as well as a spontaneous lattice strain at the transition point [48,49]. Again, we suggest the scarcity of a purely second-order ferromagnetic (ferrimagnetic) transition, as long as the inevitable coupling between the magnetization and the crystal lattice exists [24].

IV. CONCLUSION

In conclusion, from the detected thermal hysteresis, latent heat, structural transition, and the Banerjee criterion, we show that the transition of TbCo₂ around 230 K is a FOPT, which can be well understood based on the Landau theory model. Moreover, our findings unify the understanding on the transition of TbCo₂: FOPT with a synchronous first-order structural transition and first-order ferrimagnetic transition. Our work may provide an insight into investigating the nature of other alleged second-order transitions for the magnetic materials that undergo both magnetic and structural transitions.

ACKNOWLEDGMENTS

The authors are grateful to Qizhong Zhao, Kang Cao, and Ruisheng Zhang for experimental assistance. This work was financially supported by the National Key Research and Development Program of China (2021YFB3501401), the National Natural Science Foundation of China (Grants No. 91963111 and No. 51601140), Key Scientific and Technological Innovation Team of Shaanxi Province (2020TD001), and Innovation Capability Support Program of Shaanxi (No.

2018PT-28 and No. 2017KTPT-04). NSF's ChemMatCARS Sector 15 is supported by the Divisions of Chemistry (CHE)

and Materials Research (DMR), National Science Foundation, under Grant No. NSF/CHE-1834750.

- [1] M. M. Vopson, *Crit. Rev. Solid State Mater. Sci.* **40**, 223 (2015).
- [2] S. L. Driver, J. Herrero-Albillos, C. M. Bonilla, F. Bartolome, L. M. Garcia, C. J. Howard, and M. A. Carpenter, *J. Phys.: Condens. Matter* **26**, 056001 (2014).
- [3] A. E. Clark and H. S. Belson, *Phys. Rev. B* **5**, 3642 (1972).
- [4] J. J. Melero and R. Burriel, *J. Magn. Magn. Mater.* **157-158**, 651 (1996).
- [5] A. E. Clark, J. R. Cullen, O. D. McMasters, and E. R. Callen, in *Magnetism and Magnetic Materials-1975*, edited by J. J. Becker, G. H. Lander, and J. J. Rhyne, AIP Conf. Proc. Vol. 29 (AIP, New York, 1976), p. 192.
- [6] S. Yang, H. Bao, C. Zhou, Y. Wang, X. Ren, Y. Matsushita, Y. Katsuya, M. Tanaka, K. Kobayashi, X. Song, and J. Gao, *Phys. Rev. Lett.* **104**, 197201 (2010).
- [7] E. Z. Valiev, *J. Exp. Theor. Phys.* **124**, 968 (2017).
- [8] K. Gu, J. Li, W. Ao, Y. Jian, and J. Tang, *J. Alloys Compd.* **441**, 39 (2007).
- [9] Y. Song, J. Chen, X. Liu, C. Wang, J. Zhang, H. Liu, H. Zhu, L. Hu, K. Lin, S. Zhang, and X. Xing, *J. Am. Chem. Soc.* **140**, 602 (2018).
- [10] J. A. Chelvane, G. Markandeyulu, N. H. Kumar, R. Nirmala, and S. K. Malik, *Phys. Rev. B* **72**, 092406 (2005).
- [11] S. Radha, S. B. Roy, A. K. Nigam, and G. Chandra, *Phys. Rev. B* **50**, 6866 (1994).
- [12] E. W. Lee and F. Pourarian, *Phys. Status Solidi A* **33**, 483 (1976).
- [13] M. Halder, S. M. Yusuf, M. D. Mukadam, and K. Shashikala, *Phys. Rev. B* **81**, 174402 (2010).
- [14] J. Herrero-Albillos, F. Bartolome, L. M. Garcia, F. Casanova, A. Labarta, and X. Batlle, *Phys. Rev. B* **73**, 134410 (2006).
- [15] S. Khmelevskiy and P. Mohn, *J. Phys.: Condens. Matter* **12**, 9453 (2000).
- [16] E. Gratz and H. Sassik, *J. Phys. F* **11**, 429 (1981).
- [17] C. M. Bonilla, J. Herrero-Albillos, F. Bartolome, L. M. Garcia, M. Parra-Borderias, and V. Franco, *Phys. Rev. B* **81**, 224424 (2010).
- [18] S. Yang, H. Bao, C. Zhou, Y. Wang, X. Ren, X. Song, Y. Matsushita, Y. Katsuya, M. Tanaka, and K. Kobayashi, *Chin. Phys. B* **22**, 046101 (2013).
- [19] S. B. Roy, *J. Phys.: Condens. Matter* **25**, 183201 (2013).
- [20] D. Huang, J. Gao, S. H. Lapidus, D. E. Brown, and Y. Ren, *Mater. Res. Lett.* **8**, 97 (2020).
- [21] C. Fang, J. Wang, F. Hong, W. D. Hutchison, M. F. Md Din, A. J. Studer, J. A. Kimpton, S. Dou, and Z. Cheng, *Phys. Rev. B* **96**, 064425 (2017).
- [22] N. Yoshimoto, J. Sakurai, and Y. Komura, *J. Magn. Magn. Mater.* **31-34**, 137 (1983).
- [23] Z. W. Ouyang, F. W. Wang, Q. Hang, W. F. Liu, G. Y. Liu, J. W. Lynn, J. K. Liang, and G. H. Rao, *J. Alloys Compd.* **390**, 21 (2005).
- [24] S. Yang, X. Ren, and X. Song, *Phys. Rev. B* **78**, 174427 (2008).
- [25] S. Yang and X. Ren, *Phys. Rev. B* **77**, 014407 (2008).
- [26] S. K. Banerjee, *Phys. Lett.* **12**, 16 (1964).
- [27] X. Zhou, W. Li, H. P. Kunkel, and G. Williams, *Phys. Rev. B* **73**, 012412 (2006).
- [28] M. Parra-Borderías, F. Bartolome, J. Herrero-Albillos, and L. M. Garcia, *J. Alloys Compd.* **481**, 48 (2009).
- [29] M. Hsini and L. Ghivelder, *Phys. B: Condens. Matter* **615**, 413055 (2021).
- [30] H. M. Rietveld, *J. Appl. Crystallogr.* **2**, 65 (1969).
- [31] R. Young, *The Rietveld Method* (Oxford University Press, Oxford, UK, 1993).
- [32] See Supplemental Material at <http://link.aps.org/supplemental/10.1103/PhysRevB.106.064409> for the deduction of the linear relation between the reciprocal susceptibility and temperature.
- [33] T. Y. Chang, C. Zhou, J. W. Mi, K. Y. Chen, F. H. Tian, Y. S. Chen, S. G. Wang, Y. Ren, D. E. Brown, X. P. Song, and S. Yang, *J. Phys.: Condens. Matter* **32**, 135802 (2020).
- [34] S. Brooker, *Chem. Soc. Rev.* **44**, 2880 (2015).
- [35] T.-H. Hsu, C.-H. Chung, F.-J. Chung, C.-C. Chang, M.-C. Lu, and Y.-L. Chueh, *Nano Energy* **51**, 563 (2018).
- [36] J. Y. Law, V. Franco, L. M. Moreno-Ramírez, A. Conde, D. Y. Karpenkov, I. Radulov, K. P. Skokov, and O. Gutfleisch, *Nat. Commun.* **9**, 2680 (2018).
- [37] D. Guo, L. M. Moreno-Ramrez, C. Romero-Muniz, Y. Zhang, J.-Y. Law, V. Franco, J. Wang, and Z. Ren, *Sci. China Mater.* **64**, 2846 (2021).
- [38] N. K. Singh, K. G. Suresh, A. K. Nigam, S. K. Malik, A. A. Coelho, and S. Gama, *J. Magn. Magn. Mater.* **317**, 68 (2007).
- [39] M. Forker, S. Muller, P. de la Presa, and A. F. Pasquevich, *Phys. Rev. B* **75**, 187401 (2007).
- [40] N. H. van Dijk, *J. Magn. Magn. Mater.* **529**, 167871 (2021).
- [41] D. Gignoux, F. Givord, and F. Sayetat, *J. Magn. Magn. Mater.* **15-18**, 1235 (1980).
- [42] M. Vazquez, W. Fernengel, and H. Kronmüller, *Physica Status Solidi A* **115**, 547 (1989).
- [43] A. M. Alsmadi, I. Bsoul, S. H. Mahmood, G. Alnawashi, K. Prokes, K. Siemensmeyer, B. Klemke, and H. Nakotte, *J. Appl. Phys.* **114**, 243910 (2013).
- [44] K. Morrison, A. Dupas, Y. Mudryk, V. K. Pecharsky, K. A. Gschneidner, A. D. Caplin, and L. F. Cohen, *Phys. Rev. B* **87**, 134421 (2013).
- [45] S. Bustingorry, F. Pomiro, G. Aurelio, and J. Curiale, *Phys. Rev. B* **93**, 224429 (2016).
- [46] J. Inoue and M. Shimizu, *J. Phys. F* **18**, 2487 (1988).
- [47] N. Duc, P. Brommer, and J. Franse, *Phys. B: Condens. Matter* **191**, 239 (1993).
- [48] C. P. Bean and D. S. Rodbell, *Phys. Rev.* **126**, 104 (1962).
- [49] O. Rice, *J. Chem. Phys.* **22**, 1535 (1954).